

## Plasticity of diamond compared to cubic BN

Zhang Su,<sup>1</sup> Chun-Xia Chi,<sup>2</sup> Xiao-Ji Weng,<sup>1</sup> Ke Tong<sup>1,\*</sup>, Xiao Dong,<sup>2</sup> Anmin Nie,<sup>1</sup> Zhisheng Zhao<sup>1</sup>,  
Xiang-Feng Zhou<sup>1,2,†</sup> and Yongjun Tian<sup>1</sup>

<sup>1</sup>Center for High Pressure Science, State Key Laboratory of Metastable Materials Science and Technology, School of Materials Science and Engineering, and School of Science, Yanshan University, Qinhuangdao 066004, China

<sup>2</sup>Key Laboratory of Weak-Light Nonlinear Photonics and School of Physics, Nankai University, Tianjin 300071, China



(Received 4 March 2023; accepted 28 June 2023; published 10 July 2023)

Owing to the same symmetry and very close lattice constants, diamond and cubic boron nitride (cBN) possess very similar physical properties, such as being superhard and brittle at ambient conditions. Here, the generalized stacking fault energy (GSFE) of different slip systems for diamond and cBN were calculated from first principles. The results show the perfect dislocation in diamond on the {100} plane dominates, while it is the {111} plane for cBN. This distinct difference originated from the saddle-shaped GSFE curve in diamond compared to the Gaussian line shape in cBN. Interestingly, the {111} slip plane of cBN remains unchanged under normal compression, while in diamond there is a transition from a {100} to {111} slip plane at a critical normal stress. This study provides an atomistic understanding of the experimental findings of room-temperature plasticity in diamond.

DOI: [10.1103/PhysRevB.108.014104](https://doi.org/10.1103/PhysRevB.108.014104)

### I. INTRODUCTION

Slip and twinning are the media for the plastic deformation of crystalline materials [1,2]. Both can be achieved through single or continuous slips of the local structure along a specific direction (known as the slip direction) on a specific plane (referred to as the slip plane) relative to the other part [3]. Previous studies have tried to gain insight into the plastic behavior of materials using their elastic properties [4–8]. For instance, it has been found that the ratio of shear modulus  $G$  to bulk modulus  $B$  is closely related to intrinsic plasticity or brittleness. Low  $G/B$  favors plasticity and vice versa, that is the famous Pugh's criterion [4]. Obviously, the plasticity of materials is an anisotropic property, so one could be led astray by inferring the plasticity of the material from these isotropic elastic properties alone. Returning to the nature of plasticity and considering the slip system (the combination of slip direction and slip plane) in plastic deformation may be a more plausible way to unveil the plasticity of materials.

Plasticity is the ability of a material to undergo permanent deformation under stress without cracking [9,10], and is essentially the response of interatomic bonding to applied stress. The composition of materials complicates interatomic bonding and leads to a variety of plastic deformations. For example, the close-packed {111} plane is the main slip plane in face-centered-cubic (fcc) metals [11–14], while either the {111} plane or the {110} plane tends to be the major operative slip system in fcc ceramics at high temperatures [15–17]. As the hardest ceramic, diamond is widely used in high-pressure physics, the machinery industry, and semiconductor

components [18–20]. Understanding the nature of plasticity in diamond has the potential to significantly enhance the reliability and lifetime of diamond tools. However, due to the brittleness of diamond, few studies have been conducted on its plasticity [21–25].

In previous studies, the plasticity deformation of diamond is observed at high temperatures (about 750–1250 °C) which is achieved by partial or perfect dislocations on the {111} slip plane [26–28]. But evidence of plasticity at room temperature is challenging [29–33]. Humble *et al.* first observed shear deformation close to the {100} plane in bulk diamond using the Knoop indenter [34], and then Eremets *et al.* also reported indirect evidence of plastic deformation in diamond anvil cell experiments [35]. Most recently, as the size of diamond decreases from bulk to the submicron and nanoscale, room-temperature dislocation plasticity has been directly observed in diamond pillars from an *in situ* mechanical test as well as molecular dynamics simulations of diamond nanoparticles [32,33,36,37]. Dislocations are activated in non-close-packed {100} planes of diamond under uniaxial compression of the ⟨111⟩ and ⟨110⟩ directions, respectively, while being activated in the {111} planes under ⟨100⟩ directional loading. Dislocation activation on the {100} plane may be attributed to the elastic instability or the emergence of a new carbon allotrope [32,33]. Alternatively, the difference in resolved shear stress applied to slip systems under uniaxial compression is also an important reason for the orientation-dependent activation of the slip plane [38–40]. However, a fundamental understanding of the intrinsic plasticity in diamond and other strong covalent crystals from the perspective of interatomic bonding is still lacking. Furthermore, it should be noted that a secondary slip system or cross-slip can be activated as internal stress accumulates during plastic deformation [41]. An example of this is the intermetallic compound Ni<sub>3</sub>Al with an  $L1_2$  structure,

\*tongke@ysu.edu.cn

†xfzhou@ysu.edu.cn

which can cross-slip from the primary  $\{111\}$  slip plane to the cube  $\{100\}$  cross-slip plane [42].

## II. METHOD

Inspired by these studies, the intrinsic slip systems of diamond and cubic boron nitride (cBN) were investigated using generalized stacking fault energy (GSFE) calculations. First-principles calculations were performed with the Vienna *ab initio* simulation package [43,44]. The electron-ion interaction was described by the projector augmented-wave method [45,46]. The local density approximation for the exchange-correlation interaction was adopted. A 48-layer-thick slab was constructed to ensure the convergence of the stacking fault energy, in which the lattice constants, topmost layer, and bottom layer were fixed during relaxation, while atomic movements normal to the slip plane of other layers were optimized. Meanwhile, a vacuum of 15 Å was adopted to avoid the interaction between the adjacent slabs. An energy cutoff of 600 eV, energy convergence of  $10^{-8}$  eV/cell, and  $13 \times 13 \times 1$   $k$ -point meshes in combination with a Gaussian smearing of 0.05 eV were chosen for the electronic self-consistency calculation. A force convergence criterion of 0.01 eV/Å was used for ionic relaxation. The elastic tensors  $c_{ij}$  of diamond and cBN were obtained by computing the second-order derivatives of total energy with respect to the position of ions using a finite-difference approach. Then, the Young's modulus  $E(hkl)$  along the  $(hkl)$  direction was calculated by anisotropic elasticity theory [47,48] using

$$1/E(hkl) = s_{11} - 2s_0[(hk)^2 + (hl)^2 + (kl)^2]/(h^2 + k^2 + l^2)^2, \quad (1)$$

$$s_{ij}c_{ijk} = \delta_{ik}, \quad (2)$$

$$s_0 = s_{11} - s_{12} - s_{44}/2, \quad (3)$$

where  $s_{ij}$  and  $\delta_{ik}$  are the compliance tensor and Kronecker  $\delta$  function, respectively.

## III. RESULTS AND DISCUSSION

In a diamond or zinc-blende structure, there are two nonequivalent families of  $\{111\}$  planes, namely, widely spaced shuffle and narrow-spaced glide planes [49]. Both shuffle and glide planes were calculated (Fig. S1 of Supplemental Material [50]) and the one with lower GSFE was plotted in Fig. 1. The GSFE curve of  $\langle 110 \rangle \{111\}$  in diamond exhibits a characteristic Gaussian distribution, while it has a saddle-shaped feature for the  $\langle 110 \rangle \{100\}$  slip system. Regardless of whether it is diamond or cBN, the energy barrier, i.e., the unstable stacking fault energy ( $\gamma_{\text{usf}}$ ) of  $\langle 110 \rangle \{100\}$ , is much lower than that of  $\langle 110 \rangle \{111\}$ , indicating that a perfect dislocation slipped on the  $\{100\}$  plane with a Burgers vector  $\mathbf{b}$  of  $1/2\langle 110 \rangle$  is energetically more favorable than that on the  $\{111\}$  plane. In most cases, the perfect dislocation on the  $\{111\}$  plane dissociates into partial dislocations with a Burgers vector  $\mathbf{b}$  of  $1/6\langle 112 \rangle$  to reduce the elastic energy of the system [45]. Thus, the GSFE of  $\langle 112 \rangle \{111\}$  was also examined. For diamond, the  $\gamma_{\text{usf}}$  of  $\langle 112 \rangle \{111\}$  is about 5.70 J/m<sup>2</sup> at  $0.50\mathbf{b}$ , which is higher than that of  $\langle 110 \rangle \{100\}$  (about

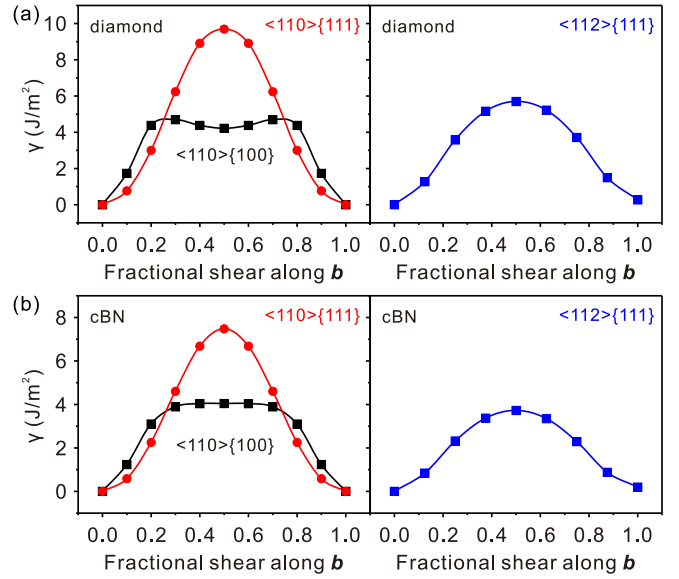


FIG. 1. Density functional theory (DFT) calculated GSFE curves for fractional shear along the  $\langle 110 \rangle$  direction on both  $\{111\}$  and  $\{100\}$  planes and the partial dislocation of  $\langle 112 \rangle \{111\}$  for (a) diamond and (b) cBN.

4.78 J/m<sup>2</sup> at  $0.26\mathbf{b}$ ). These results clearly demonstrate the preference for plastic deformation on  $\{100\}$  planes in the form of perfect dislocations in diamond, which is consistent with previous experimental and theoretical results [32,36,37]. However, the situation is quite different for cBN. In this case, the  $\gamma_{\text{usf}}$  of  $\langle 112 \rangle \{111\}$  is 0.2 J/m<sup>2</sup> lower than that of  $\langle 110 \rangle \{100\}$ . Thus, in terms of cBN, partial dislocations are the prevailing means of plastic deformation, which is consistent with the conventional understanding of metal plasticity [3,11–14].

The distinct intrinsic plasticity between diamond and cBN motivates us to explore the underlying physics on an atomic level. Figures 2(a) and 2(b) illustrate the respective atomic motions when plastic deformation arises on  $\langle 110 \rangle \{100\}$  and  $\langle 112 \rangle \{111\}$  slip systems. For the  $\langle 110 \rangle \{100\}$  system, we assume that atoms A and B are movable, and the bond angle AOD and the dihedral angle between plane AOD and plane COD are examined. Correspondingly, for the  $\langle 112 \rangle \{111\}$  system, atoms A, B, and C are assumed to be mobile, and the bond angle AOB and the dihedral angle between plane AOB and plane AOD are examined. Furthermore, the bond length AO is calculated in both cases. Since the lattice constant of cBN ( $\sim 3.58$  Å) is larger than that of diamond ( $\sim 3.53$  Å), the bond lengths of cBN are always longer than that of diamond before plastic deformation, as shown in Figs. 2(c) and 2(d). The bond length AO gradually shortens with the emergence of plastic deformation. A longer bond length of cBN than diamond is consistently observed throughout the deformation on the  $\langle 112 \rangle \{111\}$  slip system. Strikingly, for the  $\langle 110 \rangle \{100\}$  slip system, the specific C-C bond lengths (AO) are abnormally increased at  $\sim 0.25\mathbf{b}$  and remain essentially unchanged above  $\sim 0.35\mathbf{b}$  while the corresponding bond lengths of cBN continue to shorten, resulting in an inversion of C-C bond length compared to that of cBN. The same conclusion can also

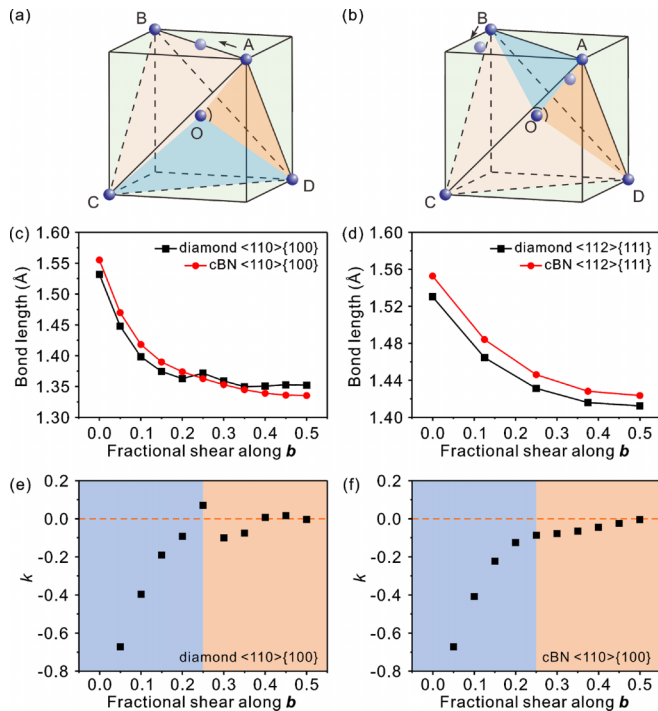


FIG. 2. Schematic diagrams of atomic motion when the slip system is (a)  $\langle 110 \rangle \{100 \}$  and (b)  $\langle 112 \rangle \{111 \}$ . Bond length of AO as a function of slip in (c)  $\langle 110 \rangle \{100 \}$  and (d)  $\langle 112 \rangle \{111 \}$  systems. Bond length change rate of AO,  $k$ , as a function of slip in (e) diamond and (f) cBN when the slip system is  $\langle 110 \rangle \{100 \}$ .

be drawn from the viewpoint of the bond length change rate  $k$  which is calculated by  $k = \Delta l / \Delta u$  where  $l$  is the bond length and  $u$  is displacement when plastic deformation occurs. As shown in Fig. 2(e), the value of  $k$  changes from negative to positive and then to negative around  $\sim 0.25b$ . Conversely, it is normal for the  $k$  curve in cBN [Fig. 2(f)]. The singularity of the  $k$  curve in diamond implies the incompressibility of interatomic bonding when plastic deformation occurs on the  $\langle 110 \rangle \{100 \}$  system. In terms of the variance of bond angle and dihedral angle, it shows an increasing tendency with the occurrence of plastic deformation (Fig. S2) of Supplemental Material [50]. No inversion similar to that in Fig. 2(c) was observed. Thus, the completely different intrinsic plasticity between diamond and cBN seems to be attributed to the inversion of the specific bond length when slipping along the  $\langle 110 \rangle$  direction on the  $\{100 \}$  plane.

In fact, the variation in bond length may be attributed to the combined effect of two factors (Fig. S3) of Supplemental Material [50]. The relative movement of two components of a material before relaxation during plastic deformation leads to a decrease in bond length AO, and the relaxation along the normal to the slip plane results in an increase in bond length AO. Thus, we tried to understand the reason behind the inversion of bond length from the perspective of relaxation along the normal to the slip plane. In Figs. 3(a) and 3(b), the gray lines mark the position of atomic planes on both sides of the slip plane. The distance between these atomic planes,  $d$ , increases as the plastic deformation occurs. To describe the variation quantitatively, the ratio of distance,

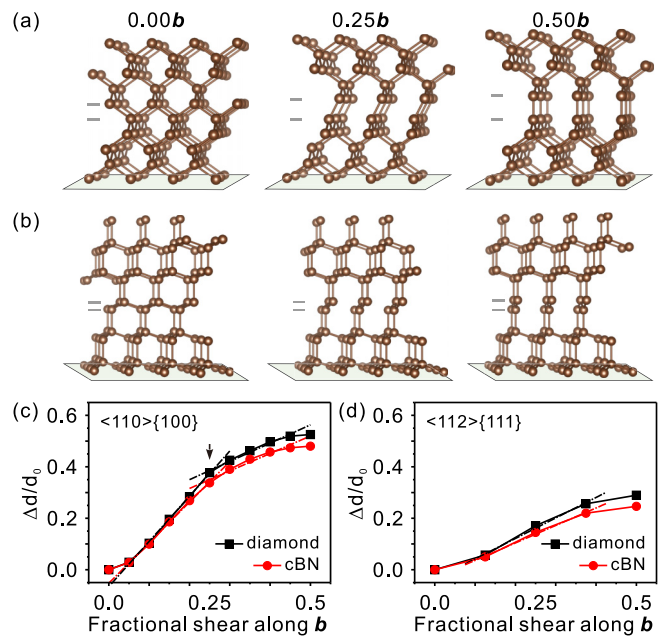


FIG. 3. Relaxed atomic structures at a slip of  $0.00b$ ,  $0.25b$ , and  $0.50b$  for (a)  $\langle 110 \rangle \{100 \}$  and (b)  $\langle 112 \rangle \{111 \}$  slip systems. The values of  $\Delta d/d_0$  as a function of slip in (c)  $\langle 110 \rangle \{100 \}$  and (d)  $\langle 112 \rangle \{111 \}$  systems. The dashed lines in (c) and (d) represent the fitting lines.

$\Delta d/d_0$  ( $\Delta d = d - d_0$ ), was calculated where  $d_0$  corresponds to the distance before plastic deformation. The results were plotted in Figs. 3(c) and 3(d). The values of  $\Delta d/d_0$  in the  $\langle 110 \rangle \{100 \}$  system are almost twice that of the  $\langle 112 \rangle \{111 \}$  system under the same amount of slip, indicating that when plastic deformation occurs in the  $\langle 112 \rangle \{111 \}$  system, the bond length reduction caused by relative movement is less. This conclusion is also consistent with Figs. 2(c) and 2(d). Considering the inversion of bond length is only observed in Fig. 2(c), it could be inferred that a sufficiently large  $\Delta d$  is the key factor for the inversion of bond length. Furthermore, for the  $\langle 110 \rangle \{100 \}$  slip system, the curve of  $\Delta d/d_0$  can be basically divided into two stages with a boundary of  $\sim 0.25b$ . In the first stage,  $\Delta d$  increases rapidly, and the slope of  $\Delta d/d_0$  curve in diamond, 1.76, is twice more than that of the second stage (0.71 for diamond). On the contrary, for the  $\langle 112 \rangle \{111 \}$  slip system, there is no sudden change for the slope of  $\Delta d/d_0$  in the range of  $\sim 0.1-0.4b$ , which may be related to the small  $\Delta d$  of the slip system. Moreover, for both slip systems, the slopes of  $\Delta d/d_0$  of diamond are always larger than that of cBN, especially for the first stage of the  $\langle 110 \rangle \{100 \}$  slip system, in which the slope of  $\Delta d/d_0$  of cBN is 1.58. The large slope of  $\Delta d/d_0$  in diamond confirms the incompressibility of C-C bonds once again. Since the bond length of diamond is hard to be further shortened after  $0.25b$ , it could be concluded that an extremely incompressible bond is another important factor for the inversion of bond length compared to cBN.

As mentioned above, the inversion of bond length depends on the relaxation along the normal to the slip plane. Obviously, it is conceivable that the  $\langle 112 \rangle \{111 \}$  slip system might become the dominant slip system of diamond again if the relaxation along the normal to the slip plane is restricted.

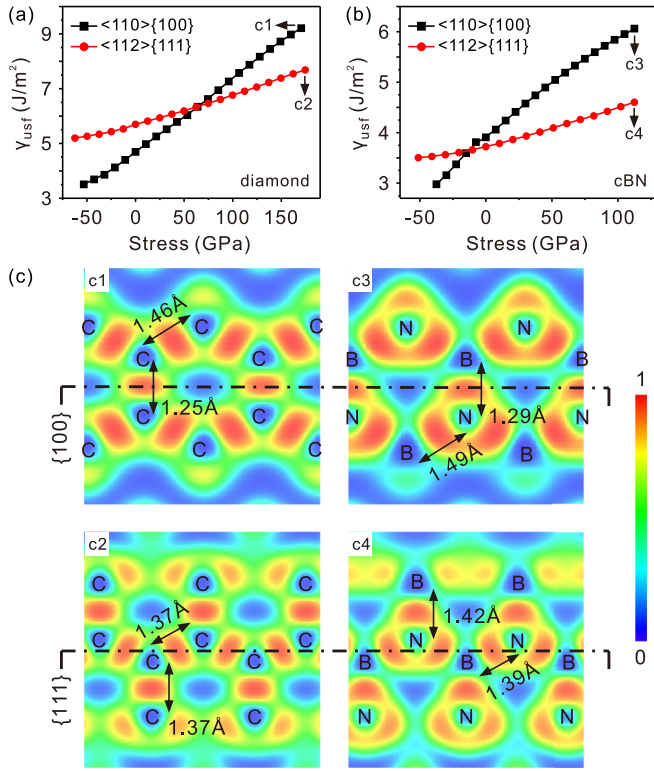


FIG. 4.  $\gamma_{\text{usf}}$  as a function of normal stress for (a) diamond and (b) cBN. The uniaxial compressive (tensile) stress expressed with a positive (negative) sign. The maximum compressive stresses for both slip systems of diamond and cBN are marked by c1, c2, c3, and c4. (c) ELF images of diamond and cBN after slipping  $0.50b$  at c1, c2, c3, and c4, respectively. The dotted lines mark the slip planes.

Previous studies also suggested that normal stress has a distinct effect on plastic deformation regardless of metals or covalent materials [51–53]. Therefore, in the following research, uniaxial compressive stress was taken into account and the results are plotted in Fig. 4. Noted that we first performed structure relaxation under normal strain to release the transverse biaxial stress, then calculated the GSFE curves on different slip systems. As compressive stress increases, the bond length gradually reduces, and  $\gamma_{\text{usf}}$  increases. In diamond, as shown in Fig. 4(a), the  $\langle 110 \rangle \{100\}$  system is energetically favorable at a stress of 0 GPa, but the  $\gamma_{\text{usf}}$  of the  $\langle 110 \rangle \{100\}$  system increases faster than that of the  $\langle 112 \rangle \{111\}$  system, thus the dominance of the  $\langle 110 \rangle \{100\}$  system gradually decreases as the stress increases, and finally the  $\langle 112 \rangle \{111\}$  system becomes more favorable after  $\sim 63.9$  GPa [Fig. 4(a) and Fig. S4] of Supplemental Material [50]. We designate this phenomenon as a stress-induced slip system flip. For comparison, the difference of  $\gamma_{\text{usf}}$  between the  $\langle 110 \rangle \{100\}$  and  $\langle 112 \rangle \{111\}$  systems in cBN increases as compressive stress increases [Fig. 4(b) and Fig. S5] of Supplemental Material

[50]. It implies that the dislocation plasticity in cBN on the  $\{111\}$  plane dominates under compressive stress. At the same time, the stress-induced slip system flip in cBN also occurs under tensile stress [Fig. 4(b)]. To study the mechanism of the stress-induced slip system flip, the electron localization function (ELF) under compressive stress was analyzed, and the results are shown in Fig. 4(c). It can be found that most of features in the ELF under large stress are the same as at 0 GPa (Fig. S6) of Supplemental Material [50], i.e., a transformation from  $sp^3$  hybridization to  $sp^2$  hybridization of carbon atoms in the vicinity of slip plane, which is identified by coordination number (3) and bond angle ( $\sim 120^\circ$ ). Furthermore, since the relaxation along the normal to the slip plane is restricted, the ELF of  $\langle 110 \rangle \{100\}$  under large stress displays a noteworthy anisotropy. Specifically, the atomic bonds perpendicular to the  $\{100\}$  slip plane are significantly shortened, resulting in the breaking of the sixfold symmetry of  $sp^2$  hybridization. For the  $\langle 112 \rangle \{111\}$  system, although the uniaxial compressive stress also restricts the relaxation along the normal to the slip plane, the sixfold symmetry of  $sp^2$  hybridization is still preserved [Figs. 4(c2) and 4(c4)]. In addition, for diamond, the elastic moduli along  $\langle 100 \rangle$  and  $\langle 111 \rangle$  directions are 1065 and 1247 GPa, respectively. Correspondingly, the elastic moduli of cBN along  $\langle 100 \rangle$  and  $\langle 111 \rangle$  are 750 and 1022 GPa, respectively. It is clear that the elastic modulus along the  $\langle 100 \rangle$  direction is lower than that along the  $\langle 111 \rangle$  direction. Thus, compared with the  $\langle 112 \rangle \{111\}$  system, the strain along the  $\langle 100 \rangle$  direction under the same stress is greater, resulting in a shorter bond length. In other words, compared with the bond length at 0 GPa, the constraint on the relaxation along the normal to the slip plane is more severe in the  $\langle 110 \rangle \{100\}$  system. These tight constraints lead to a rapid increase in  $\gamma_{\text{usf}}$  with increasing stress and the stress-induced flip in the  $\langle 110 \rangle \{100\}$  system of diamond.

#### IV. CONCLUSION

In summary, the plasticity of diamond and cBN was systematically investigated based on the GSFE curves associated with the variance of bond length. It revealed that the perfect dislocation on the  $\{100\}$  plane is dominant in diamond while the partial dislocation on the  $\{111\}$  plane is the prevailing pattern of plastic deformation in cBN. The activation of the non-close-packed  $\{100\}$  plane in diamond is attributed to the unusual variance of bond length due to the compromise between shear deformation and normal relaxation. These results shed light on the non-close-packed slip plane of diamond.

#### ACKNOWLEDGMENTS

This work was supported by the National Natural Science Foundation of China (Grants No. 52025026 and No. 52090020), and the National Key R&D Program of China (Grant No. 2018YFA0305900).

[1] D. R. Askeland, P. P. Phulé, W. J. Wright, and D. K. Bhattacharya, *The Science and Engineering of Materials* (Springer, Dordrecht, 2003).

[2] W. D. Callister and D. G. Rethwisch, *Materials Science and Engineering: An Introduction* (Wiley, New York, 2018).

- [3] Y. T. Zhu, X. Z. Liao, and X. L. Wu, Deformation twinning in nanocrystalline materials, *Prog. Mater. Sci.* **57**, 1 (2012).
- [4] S. F. Pugh, Relations between the elastic moduli and the plastic properties of polycrystalline pure metals, *London, Edinburgh Dublin Philos. Mag. J. Sci.* **45**, 823 (1954).
- [5] J. J. Lewandowski, W. H. Wang, and A. L. Greer, Intrinsic plasticity or brittleness of metallic glasses, *Philos. Mag. Lett.* **85**, 77 (2005).
- [6] S. J. Poon, A. Zhu, and G. J. Shiflet, Poisson's ration and intrinsic plasticity of metallic glasses, *Appl. Phys. Lett.* **92**, 261902 (2008).
- [7] Y.-P. Wang, G.-Y. Gan, W. Wang, Y. Yang, and B.-Y. Tang, *Ab initio* prediction of mechanical and electronic properties of ultrahigh temperature high-entropy ceramics  $(\text{Hf}_{0.2}\text{Zr}_{0.2}\text{Ta}_{0.2}\text{M}_{0.2}\text{Ti}_{0.2})\text{B}_2$  ( $M = \text{Nb}, \text{Mo}, \text{Cr}$ ), *Phys. Status Solidi B* **255**, 1800011 (2018).
- [8] D. G. Sangiovanni, W. Mellor, T. Harrington, K. Kaufmann, and K. Vecchio, Enhancing plasticity in high-entropy refractory ceramics via tailoring valence electron concentration, *Mater. Des.* **209**, 109932 (2021).
- [9] J. Lubliner, *Plasticity Theory* (Courier Corporation, North Chelmsford, MA, 2008).
- [10] D. Bigoni, *Nonlinear Solid Mechanics: Bifurcation Theory and Material Instability* (Cambridge University Press, Cambridge, U.K., 2012).
- [11] J. P. Hirth and J. Lothe, *Theory of Dislocations*, 2nd ed. (Wiley, New York, 1982).
- [12] J. E. Field and C. J. Freeman, Strength and fracture properties of diamond, *Philos. Mag. A* **43**, 595 (1981).
- [13] C. P. Frick, B. G. Clark, S. Orso, A. S. Schneider, and E. Artz, Size effect on strength and strain hardening of small-scale [111] nickel compression pillars, *Mater. Sci. Eng., A* **489**, 319 (2008).
- [14] M. Jahnátek, J. Hafner, and M. Krajčí, Shear deformation, ideal strength, and stacking fault formation of fcc metals: A density-functional study of Al and Cu, *Phys. Rev. B* **79**, 224103 (2009).
- [15] N. De Leon, X. X. Yu, H. Yu, C. R. Weinberger, and G. B. Thompson, Bonding Effects on the Slip Differences in the B1 Monocarbides, *Phys. Rev. Lett.* **114**, 165502 (2015).
- [16] H. Kindlund, D. G. Sangiovanni, I. Petrov, J. E. Greene, and L. Hultman, A review of the intrinsic ductility and toughness of hard transition-metal nitride alloy thin films, *Thin Solid Films* **688**, 137479 (2019).
- [17] R. E. Tressler and R. C. Bradt, *Deformation of Ceramic Materials II* (Springer, Berlin, 2012).
- [18] R. H. Wentorf, R. C. Devries, and F. P. Bundy, Sintered superhard materials, *Science* **208**, 873 (1980).
- [19] J. Isberg, J. Hammersberg, E. Johansson, T. Wikstrom, D. J. Twitchen, A. J. Whitehead, S. E. Coe, and G. A. Scarsbrook, High carrier mobility in single-crystal plasma-deposited diamond, *Science* **297**, 1670 (2002).
- [20] H. K. Mao, X. J. Chen, Y. Ding, B. Li, and L. Wang, Solids, liquids, and gases under high pressure, *Rev. Mod. Phys.* **90**, 015007 (2018).
- [21] M. N. R. Ashfold, J. P. Goss, B. L. Green, P. W. May, M. E. Newton, and C. V. Peaker, Nitrogen in diamond, *Chem. Rev.* **120**, 5745 (2020).
- [22] B. Li, H. Sun, and C. Chen, Extreme Mechanics of Probing the Ultimate Strength of Nanotwinned Diamond, *Phys. Rev. Lett.* **117**, 116103 (2016).
- [23] C. Liu, X. Song, Q. Li, Y. Ma, and C. Chen, Smooth Flow in Diamond: Atomistic Ductility and Electronic Conductivity, *Phys. Rev. Lett.* **123**, 195504 (2019).
- [24] C. Liu, X. Song, Q. Li, Y. Ma, and C. Chen, Superconductivity in Compression-Shear Deformed Diamond, *Phys. Rev. Lett.* **124**, 147001 (2020).
- [25] C. R. Miranda, A. Antonelli, and R. W. Nunes, Stacking-Fault Based Microscopic Model for Platelets in Diamond, *Phys. Rev. Lett.* **93**, 265502 (2004).
- [26] T. Evans and R. K. Wild, Plastic bending of diamond plates, *Philos. Mag.* **12**, 479 (1965).
- [27] C. A. Brookes and E. J. Brookes, Diamond in perspective: a review of mechanical properties of natural diamond, *Diamond Relat. Mater.* **1**, 13 (1991).
- [28] A. Mussi, D. Eyidi, A. Shiryayev, and J. Rabier, TEM observations of dislocations in plastically deformed diamond, *Phys. Status Solidi A* **210**, 191 (2013).
- [29] A. T. Blumenau, M. I. Heggie, C. J. Fall, R. Jones, and T. Frauenheim, Dislocations in diamond: Core structures and energies, *Phys. Rev. B* **65**, 205205 (2002).
- [30] A. T. Blumenau, R. Jones, T. Frauenheim, B. Willems, O. I. Lebedev, G. Van Tendeloo, D. Fisher, and P. M. Martineau, Dislocations in diamond: Dissociation into partials and their glide motion, *Phys. Rev. B* **68**, 014115 (2003).
- [31] J. Fuller and Q. An, Room-temperature plastic deformation in diamond nanopillars, *Matter* **2**, 1082 (2020).
- [32] A. Nie, Y. Bu, J. Huang, Y. Shao, Y. Zhang, W. Hu, J. Liu, Y. Wang, B. Xu, Z. Liu *et al.*, Direct observation of room-temperature dislocation plasticity in diamond, *Matter* **2**, 1222 (2020).
- [33] B. Regan, A. Aghajamali, J. Froech, T. T. Tran, J. Scott, J. Bishop, I. Suarez-Martinez, Y. Liu, J. M. Cairney, N. A. Marks *et al.*, Plastic deformation of single-crystal diamond nanopillars, *Adv. Mater.* **32**, 1906458 (2020).
- [34] P. Humble and R. H. J. Hannink, Plastic deformation of diamond at room temperature, *Nature (London)* **273**, 37 (1978).
- [35] M. I. Eremets, I. A. Trojan, P. Gwaze, J. Huth, R. Boehler, and V. D. Blank, The strength of diamond, *Appl. Phys. Lett.* **87**, 141902 (2005).
- [36] Y. Bu, P. Wang, A. Nie, and H. Wang, Room-temperature plasticity in diamond, *Sci. China: Technol. Sci.* **64**, 32 (2021).
- [37] G. Garcia Vidable, R. I. Gonzalez, F. J. Valencia, N. Amigo, D. Tramontina, and E. M. Bringa, Simulations of plasticity in diamond nanoparticles showing ultrahigh strength, *Diamond Relat. Mater.* **126**, 109109 (2022).
- [38] S. Kiani, C. Ratsch, A. M. Minor, J. M. Yang, and S. Kodambaka, In situ transmission electron microscopy observations of room-temperature plasticity in sub-micron-size TaC (100) and TaC (011) single crystals, *Scr. Mater.* **100**, 13 (2015).
- [39] S. Kiani, J. M. Yang, S. Kodambaka, and D. J. Green, Nanomechanics of refractory transition-metal carbides: A path to discovering plasticity in hard ceramics, *J. Am. Ceram. Soc.* **98**, 2313 (2015).
- [40] C. Liang, K. Tong, J. Huang, Y. Bu, J. Liu, Z. Zhao, L. Wang, B. Xu, Z. Liu, Y. Wang *et al.*, Extreme dislocation-mediated plasticity of yttria-stabilized zirconia, *Mater. Today Phys.* **22**, 100588 (2022).

- [41] W. Püschl, Models for dislocation cross-slip in close-packed crystal structures: a critical review, *Prog. Mater. Sci.* **47**, 415 (2002).
- [42] V. Paidar, D. P. Pope, and V. Vitek, A theory of the anomalous yield behavior in  $L1_2$  ordered alloys, *Acta Metall.* **32**, 435 (1984).
- [43] G. Kresse and J. Hafner, *Ab initio* molecular dynamics for liquid metals, *Phys. Rev. B* **47**, 558 (1993).
- [44] G. Kresse and J. Furthmüller, Efficient iterative schemes for *ab initio* total-energy calculations using a plane-wave basis set, *Phys. Rev. B* **54**, 11169 (1996).
- [45] P. E. Blöchl, Projector augmented-wave method, *Phys. Rev. B* **50**, 17953 (1994).
- [46] G. Kresse and D. Joubert, From ultrasoft pseudopotentials to the projector augmented-wave method, *Phys. Rev. B* **59**, 1758 (1999).
- [47] J. F. Nye, *Physical Properties of Crystals* (Clarendon Press, Oxford, U.K., 1985).
- [48] J. M. Zhang, Y. Zhang, K. W. Xu, and V. Ji, Young's modulus surface and Poisson's ratio curve for cubic metals, *J. Phys. Chem. Solids* **68**, 503 (2007).
- [49] L. Pizzagalli and P. Beauchamp, Dislocation motion in silicon: the shuffle-glide controversy revisited, *Philos. Mag. Lett.* **88**, 421 (2008).
- [50] See Supplemental Material at <http://link.aps.org/supplemental/10.1103/PhysRevB.108.014104> for additional calculations and electronic properties.
- [51] P. Andric, B. Yin, and W. A. Curtin, Stress-dependence of generalized stacking fault energies, *J. Mech. Phys. Solids* **122**, 262 (2019).
- [52] Y. Umeno and M. Černý, Effect of normal stress on the ideal shear strength in covalent crystals, *Phys. Rev. B* **77**, 100101 (2008).
- [53] J. Pokluda, M. Černý, M. Šob, and Y. Umeno, *Ab initio* calculations of mechanical properties: Methods and applications, *Prog. Mater. Sci.* **73**, 127 (2015).